Bin-Bin Xu[1]
Zhuo-Chen Ma[1]
Huan Wang[1]
Xue-Qing Liu[1]
Yong-Lai Zhang[1]*
Xu-Lin Zhang[1]
Ran Zhang[1]
Hao-Bo Jiang[1]
Hong-Bo Sun[1,2]

[1]State Key Laboratory on Integrated Optoelectronics, College of Electronic Science and Engineering, Jilin University, Changchun, P. R. China
[2]College of Physics, Jilin University, Changchun, P. R. China

Received June 12, 2011
Revised August 4, 2011
Accepted August 6, 2011

Research Article

A SERS-active microfluidic device with tunable surface plasmon resonances

A surface-enhanced Raman scattering (SERS)-active microfluidic device with tunable surface plasmon resonances is presented here. It is constructed by silver grating substrates prepared by two-beam laser interference of photoresists and subsequent metal evaporation coating, as well as PDMS microchannel derived from soft lithography. By varying the period of gratings from 200 to 550 nm, surface plasmon resonances (SPRs) from the metal gratings could be tuned in a certain range. When the SPRs match with the Raman excitation line, the highest enhancement factor of 2×10^7 is achieved in the SERS detection. The SERS-active microchannel with tunable SPRs exhibits both high enhancement factor and reproducibility of SERS signals, and thus holds great promise for applications of on-chip SERS detection.

Keywords:
Laser / Microfluidics / SERS / Silver grating / SPRs DOI 10.1002/elps.201100309

1 Introduction

Recent advancements in chemical analysis, biomedicine, food safety inspection, environmental or metabolite detection continue to stimulate the demand for information collection by using multiplex technologies in the manner of smaller sample consumption, shorter reaction time, higher sensitivity and lower cost [1–4]. Notably, microchip-based detection-analysis system is considered as a promising candidate to reach this goal due to its distinct advantages such as low dosage, environmental friendliness, high safety and sensitivity. Till now, multiform detecting methods including LIF, UV–visible absorption, chemiluminescence and biosensor have been successfully applied into microfluidic systems [5–11]. With the help of these spectral analyses, highly sensitive detections of various analytes were successfully performed inside a microfluidic device. For instance, the combination of LIF technique and microfluidic system could realize single molecule detection when the probing molecule has typical fluorescence.

As an efficient spectroscopic analysis technique, surface-enhanced Raman scattering (SERS) detection has attracted much attention due to its strong capability to provide structural information about probing molecules and highly sensitive detection at the single molecule level [12–15]. SERS is so fascinating that Raman signals could be enormously increased by a factor of million or even higher compared with normal signals. Based on this amplified detection, various SERS sensors have been proved effective for a wide range of analytes. For example, SERS measurements performed on yeast cells and citrus fruits with pesticide residues illustrate the potential applications in life sciences, especially for the inspection of food safety and environment pollutants [16]. Additionally, SERS spectrum can effectively monitor the environmental pH change when the probe molecules have certain pH dependence, and thus it could act as a sensor to image pH values in the endosomal compartments of single cells [17], further demonstrating its great potential in the materials and life sciences.

To date, the combination of SERS-active substrates with microfluidic devices shows promising capability for highly sensitive on-chip detection of various analytes, especially biomolecules. [18–20] For example, Gamby et al. reported a gold nanowires embellished polycarbonate microchannel as a SERS-active device [18]; Lee et al. showed lable-free biomolecular detection by using SERS-active electrodes [19]; Chang et al. reported an on-chip SERS analysis of bacteria based on a roughened metal surface [20]. However, most of these SERS-active substrates were post-integrated inside a microchannel through various approaches, and the fundamental concept is to fabricate a rough metallic surface within a microchannel. At present, it is still challenging to fabricate SERS-active microfluidic devices based on general chips, for instance, PDMS channel. Although some previous works have shown the SERS detection inside a microfluidic channel by using silver and gold colloids as reproducible

Correspondence: Professor Hong-Bo Sun, College of Electronic Science and Engineering, Jilin University, Changchun 130012, P. R. China
E-mail: hbsun@jlu.edu.cn
Fax: +86-431-85168281

Abbreviations: AFM, atomic force microscopy; **EF,** enhancement factor; **p-ATP,** *p*-aminothiophenol; **R6G,** Rhodamine 6G; **SERS,** surface-enhanced Raman scattering; **SPs,** surface plasmons; **SPRs,** surface plamons resonances

*Additional corresponding author: Dr. Yong-Lai Zhang
E-mail: yonglaizhang@jlu.edu.cn

Colour online: See the article online to view Figs. 1–6 in colour.

SERS-active substrate in segmented flow [21, 22], there are still a lot of problems for practical microfluid analysis including compatibility, enhanced efficiency and sensitivity. To gain the highest SERS enhancement, a SERS-active substrate with tunable surface plasmon resonances to match the exciting laser is highly desired. However, to the best of our knowledge, SERS-active microfluidic channel with tunable SERS enhancement is still a challenging task for Lab-on-a-Chip system.

In this work, we demonstrate a fabrication of SERS-active microfluidic device with tunable surface plasmon resonances (SPRs). Typically, silver grating substrates with adjustable periods were fabricated through two-beam laser interference of photoresists and subsequent metal evaporation technologies. After coating a soft lithography-derived PDMS microchannel to the silver grating substrates, a SERS-active microfluidic device was finally achieved. This SERS microchannel exhibits high average enhancement factor (EF) and high point-to-point reproducibility, which thereby has more uniform hotspots and brings fewer disturbances to analytes compared with colloid-based SERS substrates. Importantly, the SPRs arised from the metal gratings could be tuned by adjusting the period of gratings and thickness of silver film to match with the Raman excitation line. The SERS spectra of probing molecules including Rhodamine 6G (R6G) and *p*-aminothiophenol (*p*-ATP) could be enhanced to as high as 10^7 with the assistance of excited SPRs.

2 Materials and methods

2.1 Preparation of grating structure

The grating substrates were fabricated by the process of two beam laser interference of photoresist. CW laser (Coherent MBD-266) with the excitation wavelength of 266 nm, a power of 70 μw and exposure time of 900 ms was used for the experiments. As shown in Scheme 1, beams were split and guided to interfere right on the interface between the photoresist layer and cover glass. Two attenuators were used to ensure an equal light intensity of two beams so as to obtain larger interfered intensity. Interference period was controlled by the angle of beams according to the following equation:

$$\Lambda = \frac{\lambda_i}{2\sin\left(\frac{\theta}{2}\right)}$$

where Λ is the period, λ_f is the laser wavelength and θ is the angle between two beams. Here, negative tone photoresist of NOA-63 was spin coated on glass or silicon substrates for the grating structuring. Gratings depth could be accurately regulated by controlling the exposure time through the optical shutter in the two-beam-interference. After the development in acetone for 60 s and a simple rinse in the same solvent, the grating structure was finally achieved.

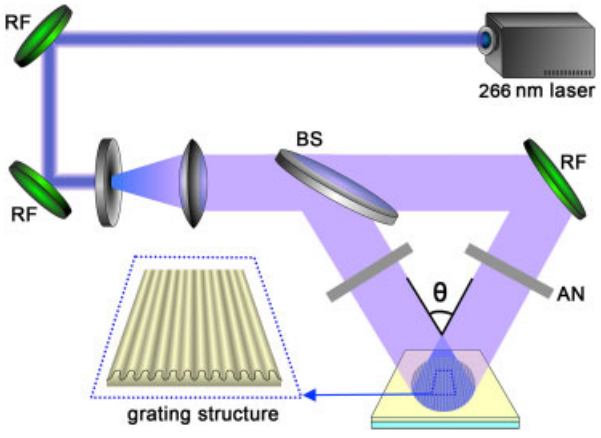

Scheme 1. Schematic illustration of two-beam interference fabrication of grating structure.

2.2 Preparation of PDMS microfluidic channel

The PDMS chip was fabricated through soft lithography technology. The SU-8 resin was spin-coated for a 50-μm thickness and the sample was prebaked for 30 min to evaporate the organic solvent. Through UV-lithography, a 50-μm high, 120-μm wide and 1-cm long template was fabricated. The template was cast with PDMS prepolymer. Subsequently, the PDMS molds were cured in a conventional drying oven at 60°C for 8 h. After the PDMS layer was peeled off, PDMS chip was obtained.

2.3 Preparation of SERS-active microfluidic devices

Scheme 2 shows the fabrication procedure of the SERS-active microfluidic devices. After two-beam-interference exposure, the substrate was immersed in acetone solution to develop, and a polymer grating substrate was achieved. Then, silver layer was evaporated on the top of the gratings (evaporation rate 0.1 nm/s in a high vacuum chamber), the thickness is fixed at 50 nm. After that, a PDMS microchannel made from soft lithography was covered onto the silver grating substrate to form a SERS-active microfluidic device. In the end, the PDMS chip was cured at 95°C for 1 h in a vacuum oven to keep tight seal.

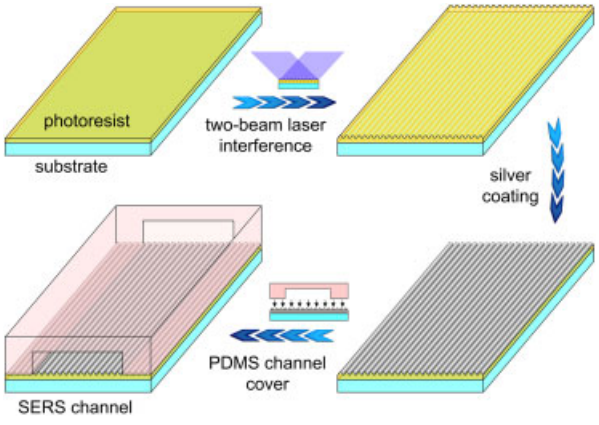

Scheme 2. Fabrication process of SERS-active microfluidic device.

2.4 Calculation of SERS EF

The calculation of SERS EF of the substrate was estimated, in order of magnitude, by the following equation [23]:

$$\mathrm{EF} = (I_{\mathrm{SERS}}/N_{\mathrm{ads}})/(I_{\mathrm{bulk}}/N_{\mathrm{bulk}}) \quad (1)$$

where I_{SERS} and I_{bulk} are the Raman signals at a certain vibration for the *p*-ATP molecules adsorbed on a substrate with SERS effect and solid *p*-ATP molecules, respectively. N_{ads} and N_{bulk} are the numbers of the adsorbed and the solid *p*-ATP molecules within the laser spot, respectively.

In our experiment, for solid *p*-ATP, the probe volume could be considered to be a tube with a waist diameter of ~1.0 μm and a depth of ~20 μm. Hence, the value of N_{bulk} is calculated to be 9.4×10^{10}. The N_{ads} can be calculated by dipping definite volume *p*-ATP/ethanol solution (0.1 μM) onto the substrate and estimating the amount of molecule in the laser dot.

2.5 Characterization and simulation

The absorption of metal gratings and metal covered bare substrates was measured by a Shimadzu UV-3600 spectrometer equipped with an integrating sphere detector. The detected spectra region is from 300 to 1000 nm. The morphologies of the microstructures were characterized by an atomic force microscopy (AFM, Veeco) in the tapping mode. SERS were measured on JOBIN YVON T64000 equipped with a liquid-nitrogen cooled argon ion laser at 514.5 nm as an excitation source (Spectra-Physics Stabilite 2017). The laser power used was about 40 μW at the samples with an average spot size of 1 μm in diameter. The spectral resolution was 4 cm^{-1} at the excitation wavelength. The probe molecules were injected into the inlet and flow past the channel using microsyringe. Subsequently, the excitation laser was focused on the SERS-active area of the chip and the SERS spectra were recorded accordingly.

The electric field component (Ex) distribution simulations of the interference field in the region of metal gratings were implemented by the finite difference time domain (FDTD) method. Just as designed structures, the polymer gratings coated with 50 nm silver film on the cover glass was used and the excitation laser used here is 514.5 nm.

3 Results and discussion

3.1 Tunable periods of silver grating

It is well known that SERS enhancement was generally explained by two typical mechanisms. One is attributed to the electromagnetic field enhancement (EFE), which accounts for the majority of the SERS signal. For the EFE mechanism, enhanced Raman scattering originates from intense electric fields in very close proximity to the SERS active surface where localized surface plasmons arise from. The electronic dynamical processes associated with SPRs can efficiently couple light in and out of the metal nanostructures when certain key structural dimensions are much smaller than the wavelength [24, 25]. The enhanced E-field can increase the Raman scattering of molecules in their vicinity by a factor of $|E|^4$ [26, 27], and thus the measured signals are enhanced in the range of 10^4–10^{15}. The other mechanism is often referred to chemical enhancement (CE), which mainly depends on the nature of the Raman analytes and SERS substrates.

Gratings as SERS substrates have a long history, mostly as objects in calculations and simulations, as well as experimental SERS substrates [28, 29]. Notably, the optical properties of nanogratings and their performance as SERS substrates depend critically on geometry. Here, we tune the enhanced E field, and thus the SPRs, by varying the periods of silver grating substrate. Generally, grating structures could be fabricated by imprint approach [30], in this work, in order to tune the period freely, two-beam-laser-interference was used to make grating structures. Figure 1 shows the AFM measurements of the silver grating surface morphologies. As a controlled experiment, a silver layer was also coated on a flat cover glass for comparison (Fig. 1A). When two-beam-laser-interference was used to pattern the photoresist substrate, grating structure was formed. AFM image of the photoresist substrate without silver coating shows that the grating structure is very uniform (Fig. 1B). The period is measured to be ~200 nm, and the depth of the grating is ~45 nm. After coating with a silver layer through evaporation, the grating structure remains clear and uniform. As shown in Fig. 1C, the period keeps the same value of ~200 nm, whereas the depth slightly decreases to ~38 nm due to the silver coating. In our experiments, both the periods and the thickness of silver layer could be tuned in a certain range. Typically, the former could be adjusted by changing the angle between two laser beams; and the later could be controlled by evaporation time. Figure 1D shows a silver grating with a period of ~280 nm. It could be clearly identified from the image that the grating is also very uniform. In this work, the period of the silver grating was tuned in the range of 200–550 nm. Here, it is worthy noting that the thickness of silver also has influence on the SERS enhancement, probably due to the difference in surface roughness. However, the resultant influence on SERS enhancement is considered to be relatively small as compared with the gating structure. Therefore, in our experiments, we only change the period of grating and the thickness of silver layer is fixed at 50 nm for comparison.

3.2 SPRs enhanced the transmission and intensity distribution of electric field component E_x

In our work, the transmission spectra of Ag grating structure and Ag film were tested on cover glass substrate when the periods of Ag grating are tuned from 200 to 550 nm, and silver thickness is fixed at 50 nm. A silver film with the same thickness is used to be compared and deducted as baseline in the final. Compared with Ag film,

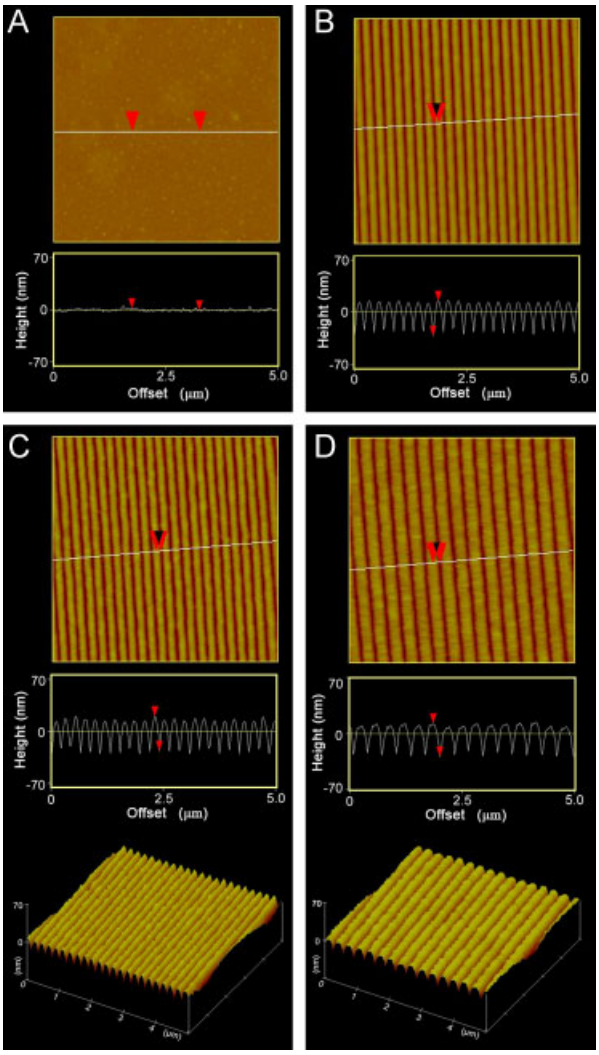

Figure 1. AFM images and height profile of (A) Ag-coated glass substrate; (B) 200 nm periodic polymer grating substrate; (C) Ag-coated ~200 nm periodic polymer grating substrate, the bottom image is the 3D view; (D) Ag-coated ~280 nm periodic polymer grating substrate, the bottom image is the 3-D view.

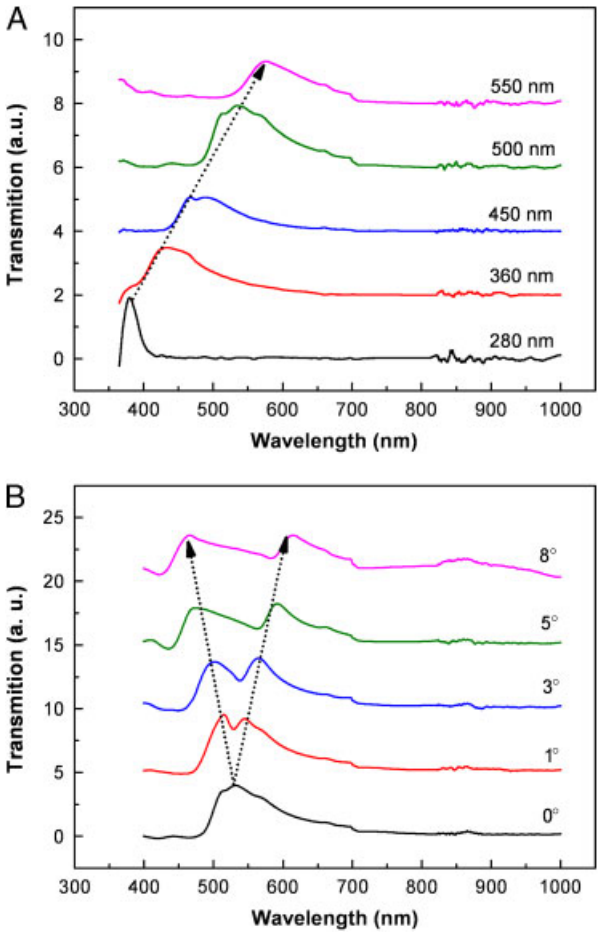

Figure 2. (A) Transmission spectra of silver grating substrate with different periods; (B) Transmission spectra of silver grating of a period of 500 nm with different incident angles.

the transmission in certain region was enhanced in the Ag grating structure. The enhanced transmission of the Ag grating structure is attributed to the surface plasmons (SPs) coupled with incident light [24, 25, 31–33]. The location of enhanced transmission band changes with the grating periods, as shown in Fig. 2A, the peaks have a red shift from 375 to 586 nm when the period changes from 280 to 550 nm. When the Ag grating has a period of 500 nm, the transmission peaked at around 520 nm which is adjacent to the Raman excitation source in our work.

In addition to the enhanced transmission, SPRs could also be identified from the splitting and shift of peaks in the opposite directions when increasing the incident angle (Fig. 2B). Such a unique transmission phenomenon is generally caused by the interaction between light and SPs. It is known that SPs are the collective oscillation of surface charges at the metal/dielectric interface [34–38], which can be excited when their wavevector matches with the incident photons and grating as follows:

$$K_{SPP} = K_0 \sin\theta \pm nK_g \quad (2)$$

where K_{SPP} is the surface plasmon polaritons wavevector, $K_0 \sin\theta = (2\pi/\lambda)\sin\theta$ is the in-plane wavevector of the incident photon, $K_g = 2\pi/\Lambda$ is the grating wavevector, Λ is the grating period and n is an integer that defines the order of the scattering process. Therefore, when the incident angle θ is varied, the incident light can excite different SPPs modes [39].

In order to obtain further insight into the local surface plasmons resonance (LSPR) influenced by different periods of Ag grating, the electric field component E_X distribution simulations of the region of metal gratings were implemented by the FDTD method. As shown in Fig. 3, the simulation of intensity distribution showed that LSPR intensity in period of 500 nm Ag grating is much stronger than that of Ag grating with a period of 280 nm when the incident laser wavelength is 514 nm. This suggests that the optical enhancement observed on silver grating surface is

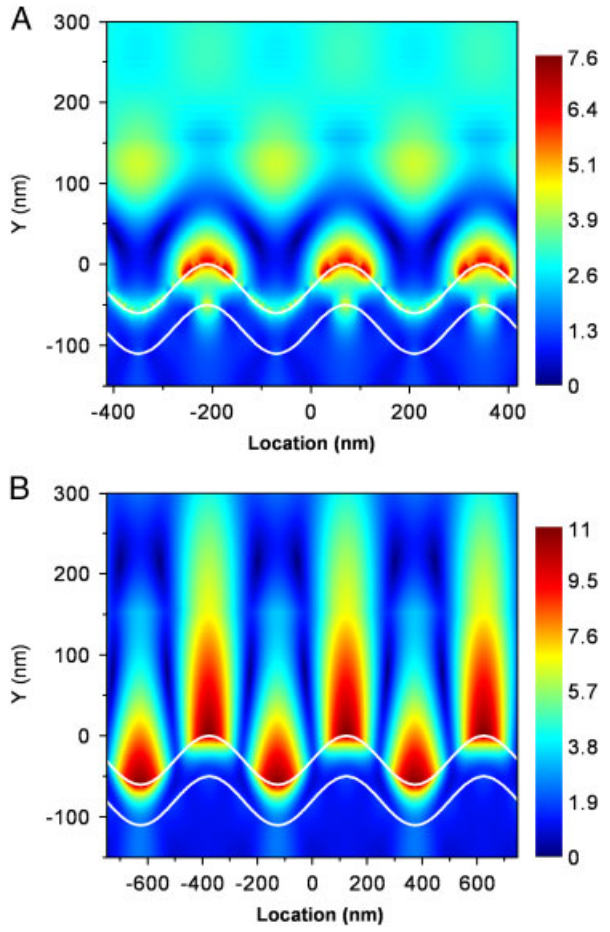

Figure 3. Electric field component E_X distribution simulations of silver grating with periods of (A) 280 nm and (B) 500 nm. The incident laser wavelength is 514 nm.

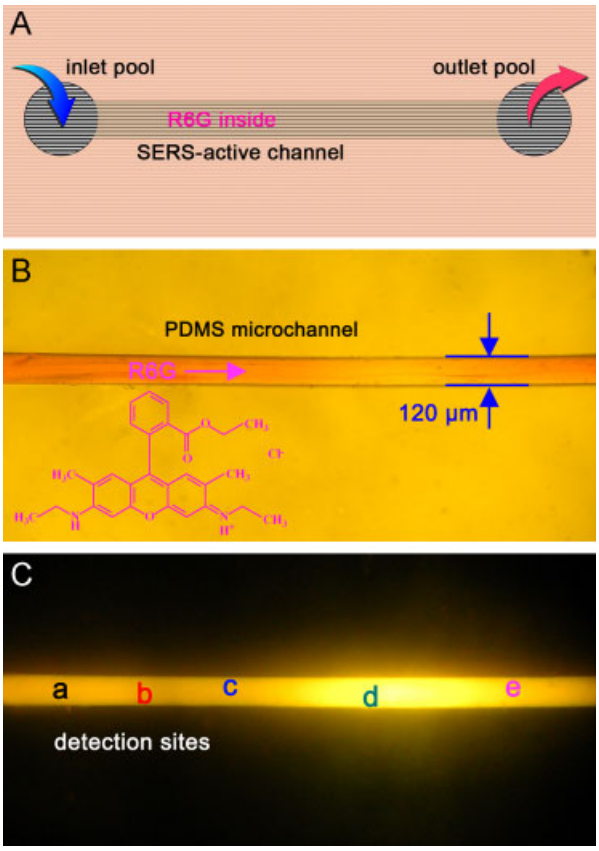

Figure 4. (A) Scheme of PDMS based SERS-active microchannel; (B) optical microscopic image of the PDMS microchannel with R6G inside, inset is the molecular structure of R6G; (C) fluorescence microscopic image of the PDMS microchannel with R6G inside, and the detection sites in the microchannel.

mainly due to the plasmons coupling, which could be tuned by variation of periodic topologies. Hence, an optimized SERS enhancement is expected when the period of Ag grating is tuned to match with the excitation source in SERS experiments.

3.3 SERS spectra

Figure 4 shows the schematic illustration of the SERS-active microfluidic channel and the optical microscopic image, as well as fluorescence microscopic image of the PDMS-based SERS microchannel. Obviously, the microchannel could be clearly identified from Fig. 4B. When R6G was injected into the microchannel, bright yellow fluorescence was observed, indicating the transparence and the interconnectivity of the PDMS channel. SERS measurement was then performed on such a microfluidic channel at different detection sites (Fig. 4C).

Figure 5 shows the SERS spectra of R6G as probing molecules. Shown in Fig. 5A is a series of SERS spectra tested in the channel with different grating periods. Notably, the strongest SERS signal of R6G is detected based on the silver grating substrate with a period of 500 nm. This result is in good agreement with the transmission spectra and the calculation results. Compared with the silver island film, the SERS signal for the silver grating substrate with 500 nm period is 10^2 times higher. Considering the roughness of silver island film, the enhancement of signal is mainly attributed to the excited SPRs and thereby enhanced optical field. Additionally, the SERS-active Ag grating substrate is uniform and has a high reproducibility. As shown in Fig. 5B, the signals of R6G detected at different sites (Fig. 4C) of the channel with period of 500 nm Ag grating are almost constant.

Figure 6 shows the SERS spectra of *p*-aminothiophenol (*p*-ATP) which is used for the calculation of the EF of our SERS-active substrate. According to the SERS spectra in Fig. 6 and Equation (2), the EF value is estimated to be 2×10^7 at the vibration of 1075 cm^{-1}, indicating the excellent performance of our SERS-active microfluidic channel (for detail of calculation, see Section 2.4).

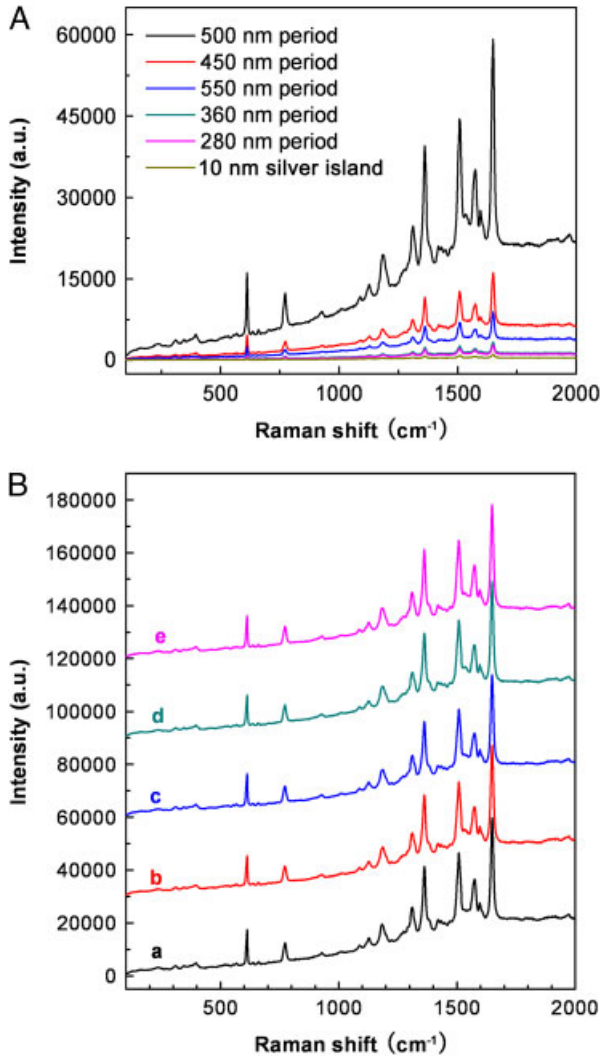

Figure 5. SERS spectra of R6G as probing molecules. (A) SERS spectra tested in the channel with different grating periods; (B) SERS spectra tested in the channel with 500 nm period at different sites (Fig. 4C).

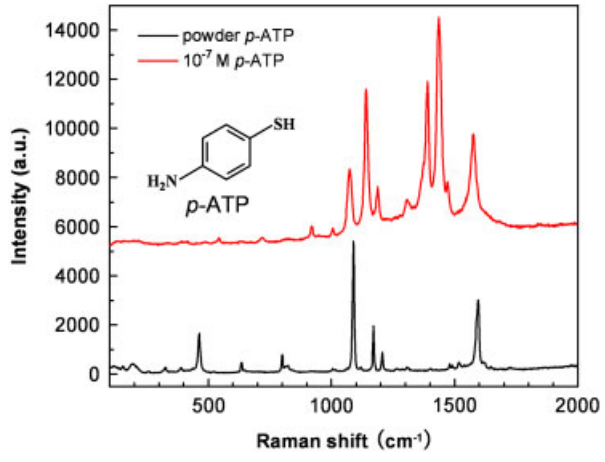

Figure 6. SERS spectra of *p*-aminothiophenol (*p*-ATP).

4 Concluding remarks

In conclusion, we have successfully fabricated a SERS-active microfluidic device with tunable surface plasmon resonances. Silver grating substrates prepared by two-beam-laser interference of photoresists and subsequent siver evaporation coating were used as tunable SERS active substrate. By varying the period of gratings from 200 to 550 nm, SPRs arised from the metal gratings was tuned to match with the Raman excitation line, so as to achieve the highest enhancement. The SERS-active substrate with a period of 500 nm shows the highest EF of 2×10^7. Both experimental and calculated results give the reason for this modulation and enhancement; that is the tunable SPRs derived from different periods could enhance the surface optical field to various extents. This SERS-active microfluidic device would find broad applications in SERS detection on a chip.

This work was supported by the financial support from NSFC under grant nos. 61008014, 60778004, 90923037, 60978062 and 60525412, and the China Postdoctoral Science Foundation No. 20110490156. The work was also supported by 2010 PhD interdisciplinary project (Jilin University) under grant no. 450091102507.

The authors have declared no conflict of interest.

5 References

[1] Huang, X., Ren, J., *Electrophoresis* 2005, *26*, 3595–3601.

[2] Ma, H., Liu, T., Qin, J., Lin, B., *Electrophoresis* 2010, *31*, 1599–1605.

[3] Viskari, P. J., Landers, J. P., *Electrophoresis* 2006, *27*, 1797–1810.

[4] Lim, T. W., Son, Y., Jeong, Y. J., Yang, D.-Y., Kong, H.-J., Lee, K.-S., Kim, D.-P., *Lab Chip* 2011, *11*, 100–103.

[5] Renzi, R. F., Stamps, J., Horn, B. A., Ferko, S., VanderNoot, V. A., West, J. A. A., Crocker, R., Wiedenman, B., Yee, D., Fruetel, J. A., *Anal. Chem.* 2004, *77*, 435–441.

[6] Tian, Y., Zhang, Y.-L., Ku, J.-F., He, Y., Xu, B.-B., Chen, Q.-D., Xia, H., Sun, H.-B., *Lab Chip* 2010, *10*, 2902–2905.

[7] Wang, J., He, Y., Xia, H., Niu, L.-G., Zhang, R., Chen, Q.-D., Zhang, Y.-L., Li, Y.-F., Zeng, S.-J., Qin, J.-H., Lin, B.-C., Sun, H.-B., *Lab Chip* 2010, *10*, 1993–1996.

[8] Zhang, Y.-L., Chen, Q.-D., Xia, H., Sun, H.-B., *Nano Today* 2010, *5*, 435–448.

[9] Xu, B.-B., Xia, H., Niu, L.-G., Zhang, Y.-L., Sun, K., Chen, Q.-D., Xu, Y., Lv, Z.-Q., Li, Z.-H., Misawa, H., Sun, H.-B., *Small* 2010, *6*, 1762–1766.

[10] DeVault, G. L., Sepaniak, M. J., *Electrophoresis* 2001, *22*, 2303–2311.

[11] Sun, K., Yamaguchi, A., Ishida, Y., Matsuo, S., Misawa, H., *Sens. Actuat. B: Chem.* 2002, *84*, 283–289.

[12] Moskovits, M., *J. Raman Spectrosc.* 2005, *36*, 485–496.

[13] Chen, L., Choo, J., *Electrophoresis* 2008, *29*, 1815–1828.

[14] Qian, X. M., Nie, S. M., *Chem. Soc. Rev.*2008, *37*, 912–920.

[15] Kneipp, K., Kneipp, H., Kneipp, J., *Acc. Chem. Res.* 2006, *39*, 443–450.

[16] Li, J. F., Huang, Y. F., Ding, Y., Yang, Z. L., Li, S. B., Zhou, X. S., Fan, F. R., Zhang, W., Zhou, Z. Y., WuDe, Y., Ren, B., Wang, Z. L., Tian, Z. Q., *Nature* 2010, *464*, 392–395.

[17] Kneipp, J., Kneipp, H., Wittig, B., Kneipp, K., *J. Phys. Chem. C* 2010, *114*, 7421–7426.

[18] Gamby, J., Rudolf, A., Abid, M., Girault, H. H., Deslouis, C., Tribollet, B., *Lab Chip* 2009, *9*, 1806–1808.

[19] Cho, H., Lee, B., Liu, G. L., Agarwal, A., Lee, L. P., *Lab Chip* 2009, *9*, 3360–3363.

[20] Cheng, I. F., Lin, C. C., Lin, D. Y., Chang, H. C., *Biomicrofluidics* 2010, *4*, 034104.

[21] Quang, L. X., Lim, C., Seong, G. H., Choo, J., Do, K. J., Yoo, S.-K., *Lab Chip* 2008, *8*, 2214–2219.

[22] Park, T., Lee, S., Seong, G. H., Choo, J., Lee, E. K., Kim, Y. S., Ji, W. H., Hwang, S. Y., Gweon, D.-G., Lee, S., *Lab Chip* 2005, *5*, 437–442.

[23] Orendorff, C. J., Gole, A., Sau, T. K., Murphy, C., *J. Anal. Chem.* 2005, *77*, 3261–3266.

[24] Ebbesen, T. W., Lezec, H. J., Ghaemi, H. F., Thio, T., Wolff, P. A., *Nature* 1998, *391*, 667–669.

[25] Søndergaard, T., Bozhevolnyi, S. I., Novikov, S. M., Beermann, J., Devaux, E., Ebbesen, T. W., *Nano Lett.* 2010, *10*, 3123–3128.

[26] Morton, S. M., Silverstein, D. W., Jensen, L., *Chem. Rev.* 2011, *111*, 3962–3994.

[27] Rycenga, M., Cobley, C. M., Zeng, J., Li, W., Moran, C. H., Zhang, Q., Qin, D., Xia, Y., *Chem. Rev.* 2011, *111*, 3669–3712.

[28] Alvarez-Puebla, R., Cui, B., Bravo-Vasquez, J.-P., Veres, T., Fenniri, H., *J. Phys. Chem. C* 2007, *111*, 6720–6723.

[29] Deng, X., Braun, G. B., Liu, S., Sciortino, P. F., Koefer, B., Tombler, T., Moskovits, M., *Nano Lett.* 2010, *10*, 1780–1786.

[30] Kim, Y., Kim, Y., Kim, S., Kim, E., *ACS Nano* 2010, *4*, 5277–5284.

[31] Genet, C., Ebbesen, T. W., *Nature* 2007, *445*, 39–46.

[32] Laux, E., Genet, C., Ebbesen, T. W., *Opt. Express* 2009, *17*, 6920–6930.

[33] Lopez-Tejeira, F., Rodrigo, S. G., Martin-Moreno, L., Garcia-Vidal, F. J., Devaux, E., Ebbesen, T. W., Krenn, J. R., Radko, I. P., Bozhevolnyi, S. I., Gonzalez, M. U., Weeber, J., Dereux, C. A., *Nat. Phys.* 2007, *3*, 324–328.

[34] Lucas, B. D., Kim, J.-S., Chin, C., Guo, L. J., *Adv. Mater.* 2008, *20*, 1129–1134.

[35] Yao, J., Le, A. P., Gray, S. K., Moore, J. S., Rogers, J. A., Nuzzo, R. G., *Adv. Mater.* 2010, *22*, 1102–1110.

[36] Ye, J., Shioi, M., Lodewijks, K., Lagae, L., Kawamura, T., Van Dorpe, P., *Appl. Phys. Lett.* 2010, *97*, 163106.

[37] Kneipp, J., Kneipp, H., McLaughlin, M., Brown, D., Kneipp, K., *Nano Lett.* 2006, *6*, 2225–2231.

[38] De Angelis, F., Das, G., Candeloro, P., Patrini, M., Galli, M., Bek, A., Lazzarino, M., Maksymov, I., Liberale, C., Andreani, L. C., Di Fabrizio, E., *Nat. Nano* 2010, *5*, 67–72.

[39] Stefan, A.M., *Plasmonics: Fundamentals and Applications*. Springer, Berlin 2007.

